Available online at www.sciencedirect.com

ScienceDirect

Scripta Materialia 80 (2014) 9–12

Scripta MATERIALIA

www.elsevier.com/locate/scriptamat

Hydrogen and aluminium in high-manganese twinning-induced plasticity steel

Do Kyeong Han,[a] Yong Min Kim,[b] Heung Nam Han,[b] H.K.D.H. Bhadeshia[a,c] and Dong-Woo Suh[a,*]

[a] *Graduate Institute of Ferrous Technology, POSTECH, Republic of Korea*
[b] *Department of Materials Science and Engineering and RIAM, Seoul National University, Republic of Korea*
[c] *Materials Science and Metallurgy, University of Cambridge, UK*

Received 23 January 2014; revised 29 January 2014; accepted 29 January 2014
Available online 8 February 2014

Given that the penetration of hydrogen into austenite is confined to surface layers following prolonged hydrogen charging, experiments were devised using nanoindentation to assess the influence of hydrogen and aluminium on the mechanical properties. It is found that the reduction in critical load for elastic to plastic transition in the hydrogen-charged layers is smaller in aluminium-alloyed steel, an effect that is not reflected in macroscopic tensile tests. The mechanism by which aluminium works to reduce hydrogen embrittlement is discussed.

Keywords: TWIP steel; Hydrogen; Aluminium; Embrittlement; Nanoindentation

Manganese-rich twinning-induced plasticity (TWIP) steels have an attractive combination of properties that are not generally matched by other advanced high-strength steels [1,2]. Some of the focus has been on a variant containing 0.6 wt.% C and 18–22 wt.% Mn with other solutes to improve weldability and enhance the resistance to hydrogen embrittlement [3–5]. Aluminium is known to mitigate delayed fracture due to hydrogen, but the underlying mechanism requires further scrutiny. The suppression of martensite during deformation, a reduction in residual stress and the formation of Al oxide at the surface have been suggested in the context of aluminium additions, but clear evidence is lacking [6–8].

There is also a complication associated with the cathodic charging of tensile specimens [6–9]; the diffusion of hydrogen in austenite is extremely slow, some six orders of magnitude slower than in ferrite at room temperature [10]. Therefore, it is only the 50–100 μm surface region that is enriched with hydrogen after prolonged charging, making it difficult to assess the outcomes of typical tensile tests. The purpose of the present work was, therefore, to study the mechanical response of hydrogen-charged TWIP steel using nanoindentation tests conducted directly on the enriched regions.

The steels investigated are Fe–0.6C–18Mn wt.% alloys containing 0 (TW1) or 1.5 wt.% Al (TW2), respectively. Cold-rolled 1 mm thick sheets were annealed at 900 °C for 15 min with heating and cooling rates of $\pm 10\ ^{\circ}C\ s^{-1}$. Metallographic samples were finish-polished with 0.25 μm diamond suspension, degreased with ethanol and characterized using a field-emission scanning electron microscope and orientation imaging. For nanomechanical measurements, the metallographically prepared samples were electropolished and etched in a solution of 10% perchloric acid and 90% of ethanol at 13.0 V for 15 min.

Electrochemical charging was conducted in an aqueous solution of 3% sodium chloride containing $0.3\ g\ l^{-1}$ ammonium thiocyanate at a cathodic current density of $5\ mA\ cm^{-2}$ for 48 h at a constant 25 °C.

* Corresponding author. Tel.: +82 542799030; fax: +82 542799299; e-mail: dongwoo1@postech.ac.kr

http://dx.doi.org/10.1016/j.scriptamat.2014.01.039
1359-6462/

To analyse the total diffusible hydrogen content after cathodic charging, a conventional thermal desorption analysis was used at a constant heating rate of 100 °C h^{-1} to a maximum temperature of 300 °C. Uniaxial tensile tests were conducted to assess the thickness of the embrittled layer via the fracture appearance. The crosshead speed was 0.03 mm s^{-1}, which corresponds to nominal strain rate of 10^{-3} s^{-1}. Nanoindents were made using a TI750 machine; the load was applied at a constant 1000 μN s^{-1} to maximum of 5000 μN. A Berkovich-type diamond tip which has a centreline-to-face angle of 65.3° was used. Generally, the movement of the indenter tip is controlled by displacement or loading rate. It is known that the displacement control is more sensitive to the material's response [11–13]. In this research, however, loading rate control was adopted to measure the strain burst pop-in during indentation precisely [14,15]. To exclude the effects due to grain boundaries, such as the orientation of the indenter tip and boundary angle, after the indentation test, Figures 1a and b were used to select indentations, excluding those that fell on grain boundaries [16–18]. The number of indentations is 49 (7 × 7 array) for the uncharged condition and 225 (15 × 15) for the charged condition. The actual numbers of selected points for analysis are 16 and 8 in TW1 and TW2 in the uncharged condition and 25 and 40 in the charged condition, respectively. Typical mechanical parameters were calculated as in Ref. [19]. The hardness is related to the maximum load, P_{max}, and projected contact area, A, as follows:

$$H = \frac{P_{max}}{A}$$

where A is a function of h_c, which is the depth of the indenter contacting with the sample. The initial part of the load–displacement curve reflects Hertzian elastic behaviour [20]:

$$P = 1.33E_r R^{0.5} h^{1.5} \quad (1)$$

where E_r is the reduced elastic modulus, which incorporates the effects of both the material and the indenter, R is the radius of the indenter tip curvature and h is the indentation depth after the test.

Representative microstructures of the steels are shown in Figures 1c and d. Orientation images revealed that both alloys are fully austenitic, with average grain sizes of 9.5 ± 1.8 and 10.5 ± 3.0 μm in TW1 and TW2, respectively, i.e. there is no significant microstructural difference due to the aluminium addition.

Figures 2a and b show the thermal desorption curves of the hydrogen-charged alloys and their macroscopic uniaxial tensile test curves with respect to the hydrogen charging. The total diffusible hydrogen was evaluated to be 0.30 and 0.42 ppmw in TW1 and TW2, respectively, consistent with previous work [21]. This does not, of course, account for the gradients that exist in the through thickness direction. Unlike other reports indicating the hydrogen embrittlement of TWIP steels [21,22], the present work finds an insignificant difference due to hydrogen, given that the total elongation of conventional austenitic TWIP steel is reported to be around 60–70% [21–24]. The reduced flow stress in the aluminium alloyed steel is as expected from previous work on uncharged samples [21].

Figure 3 shows the fracture surface of hydrogen-charged alloys. For both steels, the brittle part of the fracture is localized to the surface layer with a thickness of ~15–20 μm. The remainder of the fracture surface is covered with ductile dimples, consistent with the fact that hydrogen does not diffuse rapidly in austenite [10]. Given that the thickness of the brittle fractured layer is similar in the TW1 and TW2 alloys but the overall hydrogen content in the TW2 alloy is high, it is presumed that the hydrogen concentration in the surface layer of TW2 is greater than in TW1. The behaviour during tensile testing involves only a small fraction of hydrogen-affected material, so the test is not sensitive to hydrogen charging.

Figures 4a and b show the load–displacement curves of the TW1 and TW2 alloys, respectively, depending on the hydrogen charging; Figures 4c and d are corresponding magnified plots and clearly show the occurrence of the first pop-in with the Hertzian elastic curves. The initial portion of loading is elastic until the first pop-in is observed [20]. The derived mechanical parameters are summarized in Table 1. The Al addition decreases the hardness but has a negligible effect on the first pop-in load. Considering that the hardness is a measure of resistance to plastic flow and the first pop-in load is related to the transition from elastic to plastic behaviour, the changes suggest that the Al addition does not

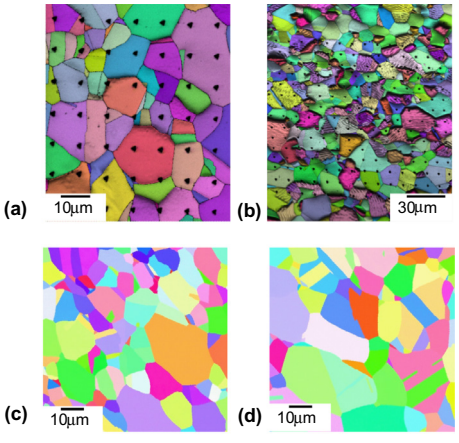

Figure 1. EBSD band contrast map of TW1 alloy after indenting (a) 7 × 7 arrays for the hydrogen uncharged and (b) 15 × 15 arrays for the hydrogen-charged condition. Typical EBSD mapping of annealed (c) TW1 and (d) TW2 alloys.

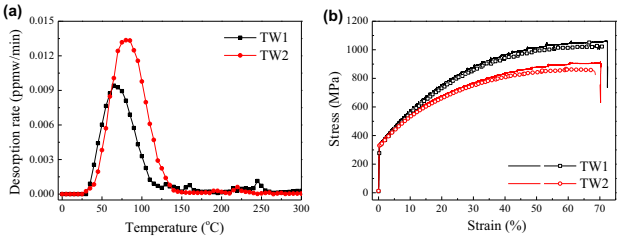

Figure 2. (a) Thermal desorption profiles with hydrogen charging and (b) stress–strain curves (symbols are uncharged and lines are charged).